Mon. Not. R. Astron. Soc. **000**, 1–10 (2014) Printed 12 September 2014 (MN LATEX style file v2.2)

Dark energy measurements with SKA HI galaxy surveys

S. Yahya[1]∗, M. Silva[2,3], M. Santos[1,2], P. Okouma[1,4,5], R. Maartens[1,6] and B. Bassett[4,5,7]

[1]*Physics Department, University of the Western Cape, Cape Town 7535, South Africa*
[2]*CENTRA, Instituto Superior Tecnico, Technical University of Lisbon, Lisboa 104900, Portugal*
[3]*Department of Physics & Astronomy, University of California, Irvine, CA 92697, USA*
[4]*African Institute for Mathematical Sciences, Muizenberg, Cape Town 7945, South Africa*
[5]*Department of Mathematics & Applied Mathematics, University of Cape Town, Cape Town 7701, South Africa*
[6]*Institute of Cosmology & Gravitation, University of Portsmouth, Portsmouth PO1 3FX, United Kingdom*
[6]*South African Astronomical Observatory, Cape Town, South Africa*

12 September 2014

ABSTRACT

We use Fisher forecasting and semi-analytical simulations of neutral hydrogen (HI) to predict the performance of Square Kilometer Array (SKA) HI galaxy surveys in measuring dark energy parameters. Measurements of the tangential and radial components of the Baryon Acoustic Oscillation (BAO) length scale over a range of redshifts are the basis for constraints on the dark energy equation of state, the rate of growth of structure and the curvature of the Universe.

Key words: cosmology : radio surveys - galaxy power spectrum - baryonic oscillations - dark energy

1 INTRODUCTION

The acoustic oscillation scale in the CMB temperature anisotropies is also imprinted in the galaxy correlations. This Baryonic Acoustic Oscillation (BAO) scale encodes the angular diameter distance $D_A(z)$ (tangential BAO scale) and the Hubble parameter $H(z)$ (radial BAO scale). One of the key science aims of the SKA is to probe dark energy via surveys of the HI galaxy distribution. These surveys will use the HI 21cm emission line (the hyperfine transition) to detect HI galaxies – detection of the line itself directly gives the redshift of the galaxy. The huge volumes that will eventually be covered by SKA HI galaxy surveys will allow for high-precision measurement of the BAO feature in the radial and tangential directions and at different cosmological redshifts.

The expected performance of these SKA surveys in constraining dark energy was investigated by (Abdalla et al. 2009). Here we update those results, using improved modeling of the number density and bias of the HI galaxy distribution.

∗E-mail:sahbayahya@gmail.com

THE SKA

The noise associated to the flux measured by the interferometer is assumed Gaussian with a r.m.s given approximately by

$$S_{\rm rms} \approx \frac{2k_B T_{\rm sys}}{A_{\rm eff}\sqrt{\delta\nu\, t_p}}, \qquad (1)$$

for an array with total effective collecting area $A_{\rm eff}$, frequency resolution $\delta\nu$ and observation time per pointing t_p (k_B is the Boltzmann constant). The computed phased array feed (PAF) beams are assumed constant across the band instead of going as λ^2 as above so that the time per pointing is also fixed. Table 1 summarizes the specifications for each telescope, and Table 2 summarizes the specifications for each survey (see Bull et al. (2014)).

2 HI GALAXY SURVEYS

For HI redshift galaxy surveys, the key inputs are (Abdalla et al. 2009) the r.m.s. sensitivity ($S_{\rm rms}$), the detection threshold (n_σ), the telescope field of view and the assumed model for HI evolution.

Telescope	Band [MHz]	z	$T_{\rm inst}$ [K]	$N_{\rm dish}$	$D_{\rm dish}$ [m]	$A_{\rm eff}$ [m^2]	Beam [deg^2] [1]	SEFD [Jy]	$S_{\rm rms}$ [μJy] [2]
ASKAP	700 - 1800[5]	(0) - 1.03	50[9]	36	12.0	3,257	30[4]	42.4	4996
MeerKAT	900 - 1670	(0) - 0.58	20	64	13.5	5,955	1.0	9.27	1093
SKA1-Sur	650 - 1670[3]	(0) - 1.19	30	60	15.0	8,482	18[4]	9.77	1151
SKA1 - Mid	950 - 1760	(0) - 0.50	20	190	15	26,189	0.75	2.1	247
SKA1-Sur+ASKAP	650 - 1670[5]	(0) - 1.19	30[5]	96	–	11,740	18[4]	9.1	832
SKA1-Mid+MK	950 - 1670	(0) - 0.50	20	254	–	32,144	0.8	1.72	202
SKA2	500 - 1200[6]	0.18 - 1.84	20	250	50[7]	400,000	30[8]	0.14	16

Table 1. Telescope configurations. [1] This is the primary beam (FoV) calculated at the center of the band. It changes as λ^2. For the combined telescopes, the smallest beam of the two telescopes is used. [2] Flux rms for a frequency interval of 0.01 MHz and 1 hour integration using eq. A3. [3] Only 500 MHz instantaneous bandwidth. [4] PAF beams assumed constant across the band. [5] Assuming that ASKAP PAFs will be replaced to meet the SKA1-Sur band and instrument temperature of 30K. Assuming that only band 2 will be initially deployed. [6] Band only indicative - can be changed. [7] These should be stations (dense aperture arrays). [8] Assuming multi-beaming to obtain large field of view.

Telescope	Band [MHz]	Beam [deg^2]	$S_{\rm area}$ [deg^2]	t_p [hours]	$S_{\rm rms}$ [μJy][4]
ASKAP[3]	700 - 1800	30	5,000	60	645
MeerKAT	900 - 1670	1.67[1]	5,000	3.34[1]	598[2]
SKA1-Sur[3]	650 - 1670	18	5,000	36	192
SKA1-Mid	950 - 1760	1.38[1]	5,000	2.76[1]	149[2]
SKA1-Sur+ASKAP[3]	700 - 1670	18	5,000	36	139
SKA1-Mid+MK	950 - 1670	1.38[1]	5,000	2.76[1]	122[2]
SKA2[3]	500 - 1200	30	30,000	10	5

Table 2. Survey specifications. We assume a total observation time of 10,000 hours. The flux rms is calculated for a frequency interval of 0.01 MHz. Values were calculated at the target frequency of 1.0 GHz, except for SKA1-Sur band 1 which has an upper limit of 900 MHz. [1] The beam and time per pointing (t_p) are assumed to change as $(\frac{1.0\,\rm GHz}{\nu})^2$ across the band. [2] The flux rms is assumed to change as $\frac{\nu}{1.0\,\rm GHz}$ across the band. [3] The beam, time per pointing and flux rms are assumed constant across the band.

2.1 HI galaxy redshift distribution

To calculate the HI galaxy number density and bias as a function of flux r.m.s, we used the S^3-SAX simulations[1]. For the detection of a galaxy, we required that at least two points on the HI line are made, that is, the width of the line has to be larger than 2× the assumed frequency resolution of the survey.

A signal to noise of 10 is then required for the detection of a galaxy.

In order to be as general as possible we didn't try to match completely the $S_{\rm rms}$ from the simulation. Instead we are giving results for several values so that a simple interpolation can be used if we decide to change the survey specs. See the appendix section B for more details.

To be able to use the simulation output at any given redshift, we use the formula of Obreschkow & Rawlings (2009) to fit the simulated dN/dz data points from S^3-SAX:

$$\frac{dN/dz}{1\rm deg^2} = 10^{c_1} z^{c_2} \exp\left(-c_3 z\right), \qquad (2)$$

where c_i are free parameters. Fig. 1 shows the fitted curves and the data points. The fitted parameters are given in Table 3.

2.2 Galaxy bias from simulation

To obtain the bias, the detected galaxies were put in a box, for which the power spectrum of the number counts was calculated. The bias squared was then taken as the ratio of that power spectrum to the dark matter one at $k = 0.2$ h/Mpc. The SAX-sky simulation consists in a mock observing cone with galaxies and their properties. This simulation was built to add HI and CO properties to the galaxies obtained by De Lucia & Blaizot (2007) using the millennium simulation with box size of 500 h^{-1} Mpc Springel et al. (2005). The galaxies are available at 64 fixed time steps from redshifts 127 to 0. In order to properly emulate the light cone, the SAX-sky simulation used only part of each box of the millennium simulation as is described in Obreschkow et al. (2009). Therefore, the boxes at fixed redshifts with HI properties which can be obtained from the SAX-sky simulation are considerable smaller than 500 h^{-1} Mpc in the line of sight direction.

The initial box for the simulation was 500 Mpc/h, but

[1] http://s-cubed.physics.ox.ac.uk/s3_sax

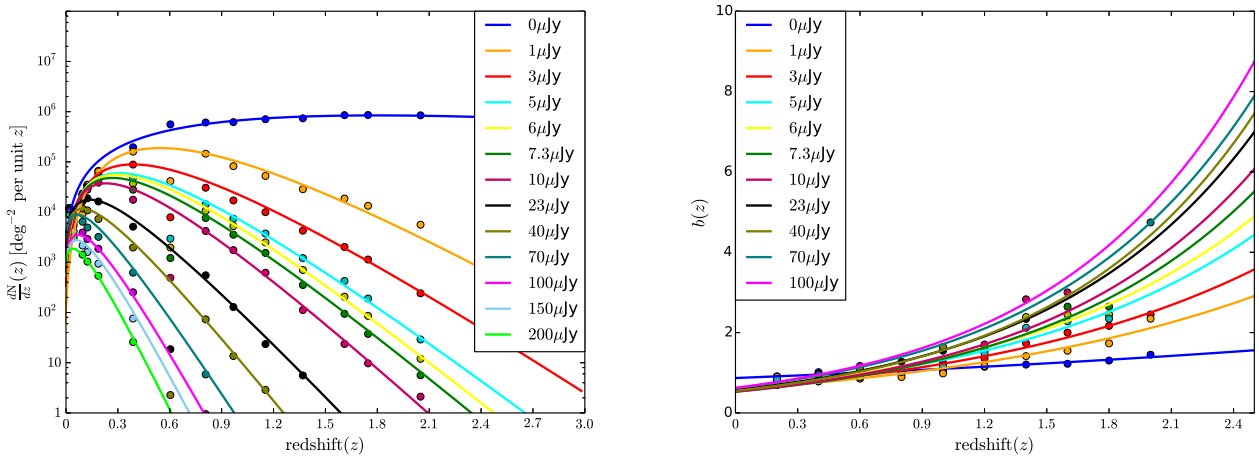

Figure 1. Upper panel: Dependence of the HI galaxy redshift distribution dN/dz (units: deg^{-2}). Note that the numbers are for different $S_{\rm rms}$ which will correspond to a given galaxy flux cut according to the procedure described in the text. Curves are the fits according to Eq. (2) and dots are from the S^3-SAX simulation. Lower Panel: HI galaxy bias for different $S_{\rm rms}$. Note that above 70 μJy values for high redshifts are purely extrapolations. However, this has little impact as at high z shot noise will dominate for these sensitivities.

Table 3. Values of the fitted parameters of Eq. (2), for different $S_{\rm rms}$.

$S_{\rm rms}$ [μJy]	c_1	c_2	c_3
0	6.21	1.63	0.90
1	7.33	3.02	5.34
3	6.91	2.38	5.84
5	6.77	2.17	6.63
6	6.84	2.23	7.13
7.3	6.76	2.14	7.36
10	6.64	2.01	7.95
23	6.02	1.43	9.03
40	5.74	1.22	10.58
70	5.62	1.11	13.03
100	5.63	1.41	15.49
150	5.48	1.33	16.62
200	5.00	1.04	17.52

Table 4. Values of the fitted parameters of Eq. (3), for different $S_{\rm rms}$.

$S_{\rm rms}$ [μJy]	c_4	c_5
0	0.8695	0.2338
1	0.5863	0.6410
3	0.6003	0.7135
5	0.5884	0.8076
6	0.5908	0.8455
7.3	0.5275	0.9385
10	0.5312	0.9745
23	0.5751	0.9993
40	0.5512	1.0417
70	0.6193	1.0179
100	0.6248	1.0554

this was further reduced along the line of sight to avoid cosmic evolution. This puts a problem on the bias extraction since we cannot efficiently use modes below $k \sim 0.1$ h/Mpc. For high flux r.m.s, the number of galaxies is low and the shot noise dominates up to very small ks. In the cosmic variance dominated case the error on the bias squared is just $\Delta b^2 \sim b^2/\sqrt{N}$ with the number of modes $N \sim [4\pi k^2 \delta k]/[(2\pi)^3/\mathrm{V}]$, δk is the k-bin used and V the volume of the box. The conclusion is that for high flux values the results should be taken as only an indication, in particular for bias above $S_{\rm rms} = 20\mu$Jy. The cosmological analysis should compare results for different fiducial values and fully marginalize over the bias and number counts. The simulated data points are shown in Fig. 1 for different $S_{\rm rms}$ sensitivities. We use an exponential function to fit a galaxy bias $b(z)$ to the simulated data:

$$b = c_4 \exp(c_5 z). \tag{3}$$

Values of the fitted parameters for each r.m.s sensitivity are given in Table 4.

2.3 Forecasting method

To predict the expected uncertainties in the cosmological parameters measured by the SKA, we use the Fisher forecasting method. The Fisher matrix is

$$F_{ij} \simeq \sum_n \frac{1}{(\Delta x_n)^2} \frac{\partial x_n}{\partial \theta_i} \frac{\partial x_n}{\partial \theta_j}, \tag{4}$$

where θ_i are the cosmological parameters, x_n are the data and Δx_n are the expected uncertainties on the data, which depend on the design of the experiment. The Fisher matrix can be expressed in terms of the observed redshift-space power spectrum P^z and the number density of galaxies n:

$$F_{ij} = \int_{-1}^{1} d\mu \int_{k_{\rm min}}^{k_{\rm max}} \frac{k^2 dk}{8\pi^2} \frac{\partial P^z}{\partial \theta_i} \frac{\partial P^z}{\partial \theta_j} \frac{V_{\rm survey}}{[P^z + n^{-1}]^2}. \tag{5}$$

The real-space power spectrum P is related to P^z by

$$P^z(k,\mu) = R(\mu,k) P(k), \tag{6}$$

$$R(\mu,k) = (1+\beta\mu^2)^2 \exp\left(-k^2\mu^2\Sigma_z^2\right). \tag{7}$$

Here $\mu = \vec{k}\cdot\vec{e}/k$, and $\vec{e}$ is the line-of-sight direction. The linear RSD parameter β is given in terms of the growth rate f by (Komatsu et al. 2009)

$$\beta(z) = \frac{f(z)}{b(z)}, \quad f(z) = -\frac{d\ln D(z)}{d\ln(1+z)}, \tag{8}$$

We obtain the growth rate by solving the differential equation of the growth (Komatsu et al. 2009).

The survey volume is given by

$$V_{\rm survey} = \left(\frac{\pi}{180}\right)^2 S_{\rm area} \int_{z_{\rm max}}^{z_{\rm min}} (1+z)^2 D_A^2(z) \frac{c}{H_0} \frac{1}{h} dz \tag{9}$$

where $V_{\rm survey}$ in units of h^{-3} Mpc^3 (Hogg 1999).

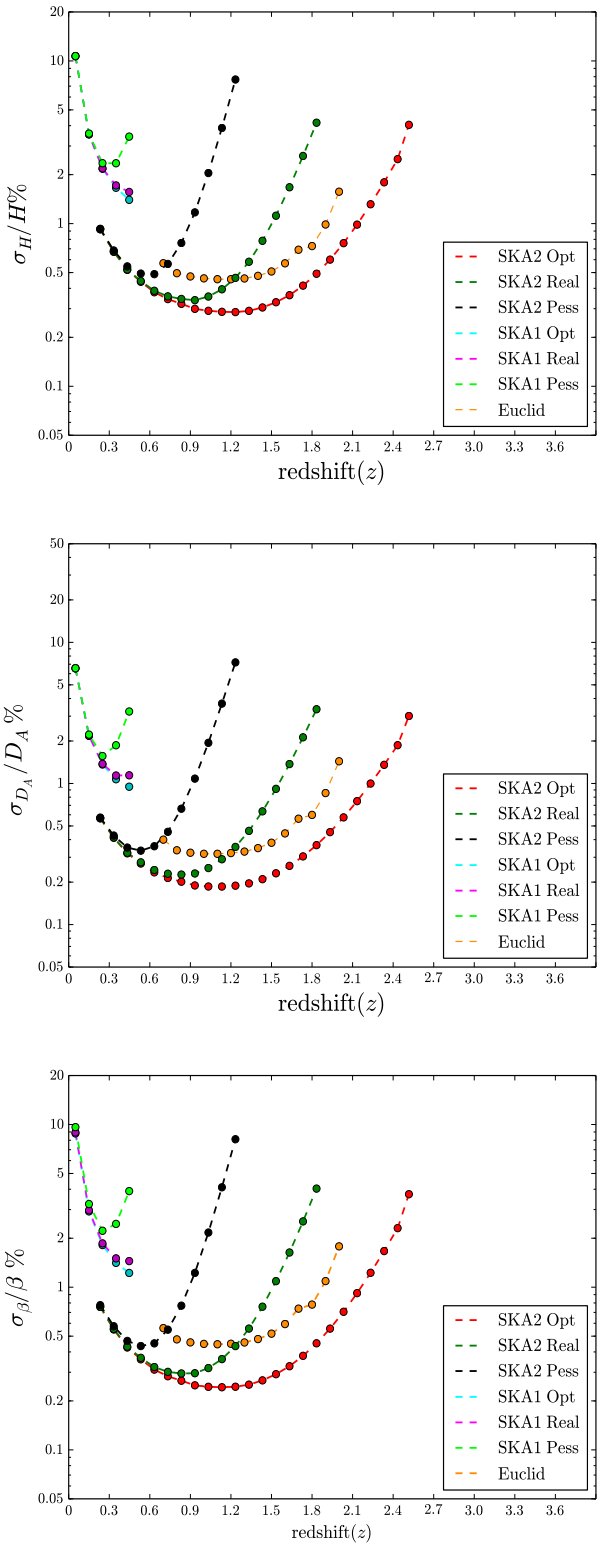

Figure 3. Top: fractional error (%) on the radial component ($\sigma_H/H\%$) . Middle: fractional error (%) on the tangential component ($\sigma_{D_A}/D_A\%$). Bottom: the fractional error (%) on β ($\sigma_\beta/\beta\%$).

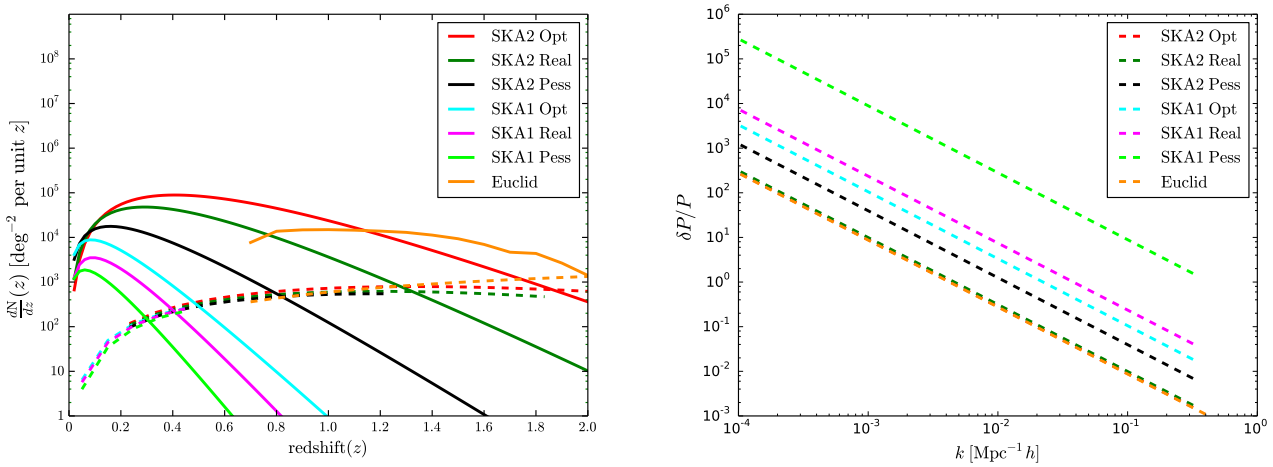

Figure 2. Left Panel: dashed lines shows the cosmic variance = shot noise for each $S_{\rm rms}$ and for Euclid redshift survey, where the solid lines shows dN/dz per unit redshift. solid lines shows dN/dz for different sensitivities and for Euclid. Right panel: shows $\delta P/P$ for different experiments.

In this work, we assume a fiducial cosmological model with cosmological parameters

$$h = 0.67,\ \Omega_{\rm cdm} = 0.316,\ \Omega_b = 0.049,\ \Omega_K = 0.0,$$
$$w_0 = -1,\ w_a = 0.0,\ n_s = 0.962. \quad (10)$$

2.3.1 Wiggles-only method

For forecasting based on the BAO, we can use a simplified approach, that has been called the wiggles-only. To construct the wiggles only power spectrum $P(k)$, using the $P(k)$ that has been produced using CAMB, we do separate the wiggles such that (Bull et al. 2014)[2]

$$f_{\rm bao}(k) = \frac{P(k) - P_{\rm ref}(k)}{P_{\rm ref}(k)} \quad (11)$$

If we assume that s is well measured from CMB observations, then the errors on $s_\perp$ and $s_\parallel$ are virtually equivalent to the errors on $D_A(z)$ and $H(z)$. We follow Seo & Eisenstein (2007) and choose

$$\theta_1 = \ln s_\perp^{-1}, \quad \theta_2 = \ln s_\parallel. \quad (12)$$

Then the Fisher matrix evaluated around the fiducial cosmology with $s_\perp = s_\parallel = s$, is given by:

$$F_{ij} = \int_{-1}^{1} d\mu \int_{k_{\rm min}}^{k_{\rm max}} \frac{k^2 dk}{8\pi^2} \frac{V_{\rm survey}}{[P^z + n^{-1}]^2} \times \left[\frac{\partial f_{\rm BAO}(k) P_{\rm ref}}{\partial k}\right]^2 \frac{\partial k}{\partial \log\theta_2} \frac{\partial k}{\partial \log\theta_1}. \quad (13)$$

[2] The Technical detail explained well on Bull et al. (2014) section IV.

2.4 Constraints on the BAO

The measurements of the BAO scale are constrained by two types of errors, cosmic variance and shot noise. Shot noise reflects the limits on reconstructing the matter distribution from galaxy surveys, and is inversely proportional to the number of galaxies at a given survey volume. Upcoming surveys such as the SKA will limit shot noise.

Cosmic variance which is the uncertainty that results from observing only part of the universe at a specific time, limits our statistical knowledge on a cosmological scale. Shot noise and cosmic variance are equal when $nP_{0.2} = 1$ (see Fig. 2).

Abdalla et al. (2009) predict that the full SKA2 survey, up to $z \sim 1.4$, will be dominated by cosmic variance. Fig. 2 shows that cosmic variance is dominant up to $z \sim 1.8$ and the effect of the bias is clear.

We also evaluate the error on the power spectrum using:

$$\left(\frac{\delta P}{P}\right)^2 = \left[V_{\rm survey} \int_{k_{min}}^{K_{max}} \frac{2\pi k^2 dk}{2(2\pi)^3} \left(1 + \frac{1}{nP_{0.2}}\right)^2\right]^{-1} \quad (14)$$

where $P_{0.2}$ is the power spectrum evaluated at $k = 0.2\ h$/Mpc, Fig. 2 show the effect of the galaxy number density and the survey volume on the errors on the power spectrum.

3 RESULTS

Our work considers the SKA, and looks at the Euclid galaxy redshift survey for comparison, we considered realistic, pessimistic and optimistic case for SKA1 and SKA2.

3.0.1 SKA

When we forecast for the SKA1, we consider different possibilities of $S_{\rm rms}$;

- 70μJy as the best case scenario,
- 100μJy as a realistic case ,
- and 200μJy as a pessimistic case.

The sky coverage area for SKA1 ~ 5000 deg^2, and for the frequency we used the frequencies for SKA1MID band (2), see Table 2. Similarly, we forecast for SKA2, with different $S_{\rm rms}$,

- 3μJy as the best case scenario,
- 7.3μJy as a realistic case,
- and 23μJy as a pessimistic case.

SKA2 will have a sky coverage of $30000\,\mathrm{deg}^2$, see Table 2.

For all cases (SKA1 and SKA2) $k_{\rm max}$ in units of $h\,\mathrm{Mpc}^{-1}$ and it evolve with redshift:

$$k_{\rm max} = k_{\rm nl}\,(1+z)^{(2/(2+n_s))} \tag{15}$$

For the minimum we choose a constant value $k_{\rm min} = 10^{-3} h\,\mathrm{Mpc}^{-1}$.

We create redshift bins between 0.1 and 2.0, and for each $S_{\rm rms}$ case the maximum redshift limit, $z_{\rm max}$ is different. $z_{\rm max}$ is set by using Table. 1 for the frquency range:

$$z_{\rm min} = \frac{\nu_{21}}{\nu_{\rm max}-1}, \quad z_{\rm max} = \frac{\nu_{21}}{\nu_{\rm min}-1} \tag{16}$$

3.0.2 Euclid

The Euclid survey is supposed to be a combination between a galaxy survey and a weak lensing survey. To compare the performance of the SKA with other upcoming surveys, we consider the Euclid redshift galaxy survey using the reference case described in Amendola et al. (2013).

3.1 Errors on D_A and $H(z)$

Using the 2×2 Fisher matrix defined in Eq. (13), the errors on $\ln D_A(z)$ and $\ln H(z)$ are computed (Seo & Eisenstein 2007):

$$\sigma_{\ln D_A} = \sqrt{(F^{-1})_{11}}, \quad \sigma_{\ln H} = \sqrt{(F^{-1})_{22}}. \tag{17}$$

In the case where the tangential and radial BAO scales are assumed to be equal, the error in $\ln R$ can be computed using (Seo & Eisenstein 2007):

$$\sigma^2_{\ln R} = \frac{\sigma^2_{\ln D_A}\left(1-r^2\right)}{1+2r\sigma_{\ln D_A}/\sigma_{\ln H}+\sigma^2_{\ln D_A}/\sigma^2_{\ln H}}, \tag{18}$$

where

$$r = \frac{F_{12}}{\sqrt{F_{11}F_{22}}}. \tag{19}$$

Fig. 3 shows the fractional percentage error on the tangential component ($\sigma_H/H\%$), the radial component ($\sigma_{D_A}/D_A\%$) and the linear RSD parameter ($\sigma_\beta/\beta\%$) for both cases SKA1 and SKA2.

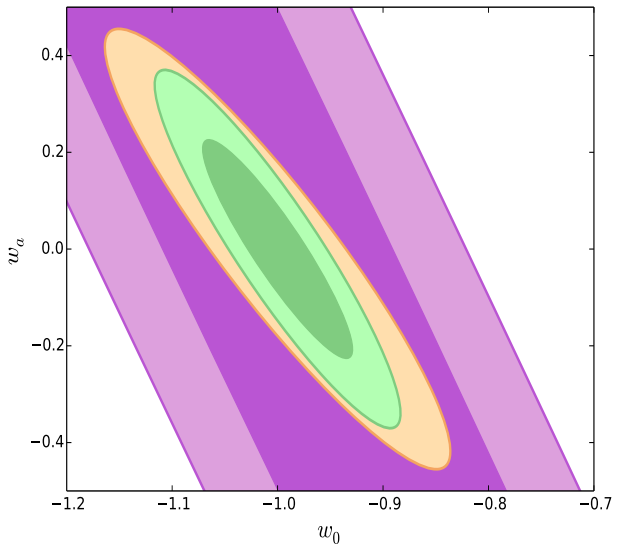

Figure 4. Projected constraints 1σ and 2σ confidence limits on the dark energy parameters w_0 and w_a for SKA1+Planck priors with $S_{\rm rms} = 100\mu$Jy (purple), SKA2+Planck priors with $S_{\rm rms} = 7.3\mu$Jy (green) and Euclid galaxy survey + Planck priors (blue).

3.2 Error propagation to β

From the uncertainty of $\ln R$ in Eq. (18), we can use the propagation of error rule to find the uncertainty of β, assuming that the error contribution from $\Sigma_z \approx 0$:

$$\sigma_\beta = \frac{(1+\mu^2\beta)^2}{2\mu^2}\sigma_{\ln R(\mu)}. \tag{20}$$

The errors in β versus redshift for different sensitivities are shown in Fig. 3.

3.3 Error propagation to dark energy equation of state

We parameterize $w(z)$ via Eq. (C6), and propagate the errors in $D_A(z)$ and $H(z)$, Eq. 5, to the cosmological parameters using:

$$\tilde{F}_{\alpha\beta} = \sum_{ij}\frac{\partial\theta_i}{\partial\theta_\alpha}\frac{\partial\theta_j}{\partial\theta_\beta}F_{ij}. \tag{21}$$

where $\theta_i = (\ln D_A, \ln H)$ and $\theta_\alpha = (w_0, w_a, \Omega_{\rm cdm}, \Omega_b, \Omega_K, h)$, for detailed calculations see Eq. D1.

Note that as prior informations about the cosmology parameters we try to estimate their uncertainity, we added Planck prior from the DETF matrix to the SKA Fisher matrix.

3.4 Figure of Merit

We define the figure of merit (FoM) as

$$\mathrm{FoM} = \sqrt{\det(F)}, \tag{22}$$

Table 5. Shows different $S_{\rm rms}$, $\sigma_{D_A}/D_A\%$ and $\sigma_H/H\%$, and the corresponding error values of w_0, w_a, $\Omega_{\rm cdm}$, Ω_b, Ω_K, h. Last column shows FoM of the SKA.

Setup	$S_{\rm rms}$ [μJy]	σ_{w_0}	σ_{w_a}	$\sigma_{\Omega_{\rm cdm}}$	σ_{Ω_b}	σ_{Ω_K}	σ_h	DETF FoM
SKA1 (5000 deg^2)	70	0.5348728	2.4161732	0.010	4.754e-04	0.01498	0.02529	6
	100	0.5484769	2.4983336	0.010	4.847e-04	0.01610	0.02564	6
	200	0.6807205	3.3121038	0.012	5.980e-04	0.02717	0.02898	3
	3	0.0311022	0.1088730	0.003	1.549e-04	0.00342	0.00309	574
SKA2 (30000 deg^2)	7.3	0.0469348	0.1490716	0.004	1.781e-04	0.00393	0.00423	357
	23	0.0958761	0.3283661	0.005	2.310e-04	0.00462	0.00699	146
SKA2 (30000 deg^2)	0 noise	0.0241942	0.0924499	0.003	1.389e-04	0.00289	0.00235	795
Euclid (15000 deg^2)	-	0.0659530	0.1832310	0.005	2.635e-04	0.00589	0.00697	209

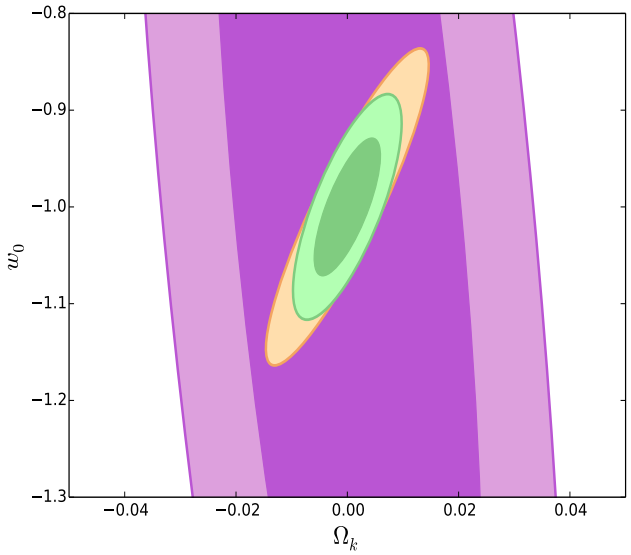

Figure 5. Projected constraints on w_0 and Ω_K, 1σ and 2σ confidence limits for the SKA1+Planck priors where $S_{\rm rms} = 100\mu$Jy (red), for the SKA2+Planck priors where $S_{\rm rms} = 7.3\mu$Jy (green) and for Euclid galaxy survey+Plank priors (blue).

which is also equivalent to the inverse of the $1-\sigma$ ellipse in units of the area of the unit circle (Bassett et al. 2011; Coe 2009).

Acknowledgements:
SY thanks Pedro Ferreira for valuable guidance, and for hospitality during her visit to Oxford University where part of this work was done. SY, MS, PO and RM are supported by the South Africa Square Kilometer Array Project and the South African National Research Foundation. RM acknowledges support from the UK Science & Technology Facilities Council (grant ST/K0090X/1).

REFERENCES

Abdalla F. B., Blake C., Rawlings S., 2009, Mon. Not. Roy. Astron. Soc., 401, 743
Amendola L., et al., 2013, Living Reviews in Relativity, 16, 6
Bassett B. A., Fantaye Y., Hlozek H R., Kotze J., 2011, International Journal of Modern Physics D, 20, 2559
Bull P., Ferreira P. G., Patel P., Santos M. G., 2014, arXiv: 1405.1452
Chevallier M., Polarski D., 2001, Int. J. Mod. Phys., D10, 213
Coe D., 2009, arXiv: 0906.4123
De Lucia G., Blaizot J., 2007, Mon. Not. Roy. Astron. Soc., 375, 2
Hogg D. W., 1999, arXiv: astro-ph/9905116
Komatsu E., et al., 2009, Astrophys.J.Suppl., 180, 330
Linder E. V., 2003, ArXiv: 0311403
Obreschkow D., Klöckner H.-R., Heywood I., Levrier F., Rawlings S., 2009, Astrophys. J., 703, 1890
Obreschkow D., Rawlings S., 2009, Astrophys. J., 703, 1890
Seo H.-J., Eisenstein D. J., 2007, Astrophys. J., 665, 14
Shoji M., Jeong D., Komatsu E., 2009, Astrophys. J., 693, 1404
Springel V., et al., 2005, Nature, 435, 629

APPENDIX A: TELESCOPE SPECIFICATIONS

Telescope sensitivities are sometimes quoted in terms of the "System Equivalent Flux Density": SEFD $\equiv 2k_{\rm B}T_{\rm sys}/A_{\rm eff}$ or just "A over ": $A_{\rm eff}/T_{\rm sys}$. The effective collecting $A_{\rm eff}$ is usually 70% to 80% of the actual array total area depending of the efficiency of the system. Note that the expression above gives the flux sensitivity per resolution beam. The equivalent brightness temperature uncertainty is

$$\sigma_T = \frac{S_{\rm rms}c^2}{2k_B\nu^2(\delta\theta)^2}, \tag{A1}$$

where $\delta\theta$ is the angular resolution of the interferometer. The total temperature is

$$T_{\rm sys} = T_{\rm inst} + T_{\rm sky} \tag{A2}$$

with $T_{\rm sky} \approx 60\,(300\,{\rm MHz}/\nu)^{2.55}$ K and $T_{\rm inst}$ the instrument temperature which is usually higher than the sky temperature above 300 MHz.

For typical instrument specifications, the single-dish noise r.m.s can be written as:

$$S_{\rm rms} = 368\,\mu{\rm Jy}\left(\frac{T_{\rm sys}}{20\,{\rm K}}\right)\times \left(\frac{25,000\,{\rm m}^2}{A_{\rm eff}}\right)\left(\frac{0.01{\rm MHz}}{\delta\nu}\right)^{1/2}\left(\frac{1{\rm h}}{t_{\rm p}}\right)^{1/2}. \tag{A3}$$

For a given survey area ($S_{\rm area}$) we will need $S_{\rm area}/(\theta_{\rm B})^2$ pointings where $(\theta_{\rm B})^2$ is the telescope field of view with the full width at half maximum of the beam, given by (in radians)

$$\theta_{\rm B} \approx \frac{1.22\lambda}{\sqrt{(A_{\rm dish})}}, \tag{A4}$$

where $A_{\rm dish}$ is the effective area of each dish. The time per pointing t_p is then related to the total integration time $t_{\rm tot}$ through

$$t_p = t_{\rm tot}\frac{(\theta_{\rm B})^2}{S_{\rm area}}. \tag{A5}$$

This will increase the time per pointing at the lowest frequencies. Note that in the table below, following what is in the SKA baseline document we use instead

$$\frac{\theta_{\rm B}}{1{\rm deg}^2} \approx \frac{\pi}{4}\left(\frac{66\lambda}{D}\right)^2. \tag{A6}$$

APPENDIX B: S^3-SAX SIMULATION

Using the S^3-SAX database, we used the following variables and prescription to detect HI galaxies:

- $z_{\rm A}$ is the apparent redshift (including Doppler correction).
- Set experiment spectral resolution to $dV = 2.1(1+z_{\rm A})$ [Km/s]. This corresponds to a frequency resolution of 0.01 [MHz] which is what has been assumed for the sensitivity calculations.
- $w_{\rm P}$ [Km/s] is line width between the two horns of the HI-line profile (already corrected for the galaxy inclination), we take only galaxies where $w_{\rm P}/2 > dV$.
- $v_{\rm HI}$ [Jy Km/s] is the velocity-integrated line flux of the HI-line, for each galaxy we get flux $= v_{\rm HI}/w_{\rm P}$ and we take only galaxies where flux $> 10\times S_{\rm rms}/\sqrt{(w_{\rm P}/dV)}$.

APPENDIX C: THEORETICAL ANALYSIS

The Hubble parameter $H(z) = H_0E(z)$ and angular diameter distance $D_A(z)$ are given by

$$E = \sqrt{\Omega_M(1+z)^3 + \Omega_K(1+z)^2 + \Omega_{\rm de}\mathcal{F}}, \tag{C1}$$

$$D_A = \frac{1}{H_0\sqrt{-\Omega_K}(1+z)}\sin\left(\sqrt{-\Omega_K}\int_0^z\frac{dz'}{E(z')}\right), \tag{C2}$$

where $\Omega_{\rm de} = 1-\Omega_M-\Omega_K$, the dark energy is described by

$$\mathcal{F}(z) = \exp\int_0^z\frac{3[1+w(z')]}{1+z'}dz', \quad w = \frac{p_{\rm de}}{\rho_{\rm de}}, \tag{C3}$$

and Ω_M is the matter density ($\Omega_{\rm cdm}+\Omega_b$).

$H(z)$ and $D_A(z)$ are related directly to the comoving size of the BAO feature along and across the line of sight:

$$s_\parallel(z) = \frac{c\Delta z}{H(z)}, \quad s_\perp(z) = (1+z)D_A(z)\Delta\theta. \tag{C4}$$

The redshift extent Δz and angular size $\Delta\theta$ of the BAO feature are the observables. In the absence of redshift-space distortions (RSD), we have

$$s_\parallel = s_\perp = s, \tag{C5}$$

where s is the comoving acoustic horizon, defined at the drag epoch. Then observations determine H and D_A separately. In order to parametrize deviations from the simplest (vacuum energy) model of DE ($w=-1$), we use (Chevallier & Polarski 2001; Linder 2003)

$$w(z) = w_0 + w_a\frac{z}{(1+z)}. \tag{C6}$$

APPENDIX D: PROPAGATION OF ERROR CALCULATIONS

Partial derivatives of D_A and H with respect to w_0 and w_a are given by (Shoji et al. 2009)

$$\begin{aligned}
\frac{\partial \ln D_A}{\partial w_0} &= -\frac{3}{2}\Omega_{\rm de}\frac{\int_0^z \ln(1+z')\mathcal{F}(z')E(z')^{-3}dz'}{\int_0^z E(z')^{-1}dz'},\\
\frac{\partial \ln D_A}{\partial w_a} &= -\frac{3}{2}\Omega_{\rm de}\\
&\times \frac{\int_0^z \left\{\ln(1+z') - \frac{z'}{(1+z')}\right\}\mathcal{F}(z')E(z')^{-3}dz'}{\int_0^z E(z')^{-1}dz'},\\
\frac{\partial \ln D_A}{\partial \Omega_{\rm cdm}} &= -\frac{1}{2}\frac{\int_0^z \left\{(1+z')^3 - \mathcal{F}(z')\right\}E(z')^{-3}dz'}{\int_0^z E(z')^{-1}dz'},\\
\frac{\partial \ln D_A}{\partial \Omega_b} &= -\frac{1}{2}\frac{\int_0^z \left\{(1+z')^3 - \mathcal{F}(z')\right\}E(z')^{-3}dz'}{\int_0^z E(z')^{-1}dz'},\\
\frac{\partial \ln D_A}{\partial \Omega_K} &= -\frac{1}{2}\frac{\int_0^z \left\{(1+z')^2 - \mathcal{F}(z')\right\}E(z')^{-3}}{\int_0^z E(z')^{-1}dz'}\\
&+ \frac{1}{6}\left(\int_0^z E(z')^{-1}dz'\right)^2,\\
\frac{\partial \ln D_A}{\partial h} &= \frac{1}{h}\\
\frac{\partial \ln H}{\partial w_0} &= \frac{3}{2}\Omega_{\rm de}\ln(1+z)\frac{\mathcal{F}(z)}{E^2(z)},\\
\frac{\partial \ln H}{\partial w_a} &= \frac{3}{2}\Omega_{\rm de}\left\{\ln(1+z) - \frac{z}{(1+z)}\right\}\frac{\mathcal{F}(z)}{g(z)},\\
\frac{\partial \ln H}{\partial \Omega_{\rm cdm}} &= \frac{1}{2}\left\{(1+z)^3 - \mathcal{F}(z)\right\}\frac{1}{E^2(z)},\\
\frac{\partial \ln H}{\partial \Omega_b} &= \frac{1}{2}\left\{(1+z)^3 - \mathcal{F}(z)\right\}\frac{1}{E^2(z)},\\
\frac{\partial \ln H}{\partial \Omega_K} &= \frac{1}{2}\left\{(1+z)^2 - \mathcal{F}(z)\right\}\frac{1}{E^2(z)},\\
\frac{\partial \ln H}{\partial h} &= -\frac{1}{h},
\end{aligned}$$

where $\mathcal{F}(z)$ and $E(z)$ are given by Eq. (C3) and (C1) respectively.

We marginalize over H_0, $\Omega_{\rm cdm}$, Ω_b and Ω_K, and we add the distance information from LSS as

$$F_{\alpha\beta}^{total}(z) = F_{\alpha\beta}^{LSS} + F_{\alpha\beta}^{gal}(z), \tag{D1}$$

where we add the angular diameter distance at $z = 1090$ using

$$F_{\alpha\beta}^{LSS} = 10^4 \frac{\partial \ln D_A(z=1090)}{\partial q_\alpha}\frac{\partial \ln D_A(z=1090)}{\partial q_\beta}. \tag{D2}$$

D0.1 Adding priors

Forecasting the errors for the cosmological parameters w_0, w_a, $\Omega_{\rm cdm}$, Ω_b, Ω_K and h, is achieved by adding a diagonal prior matrix, derived from Plank's prior matrix (Amendola et al. 2013), to the SKA Fisher matrix, see Table D0.1.

We also add prior information about the angular diameter distance out to $z = 1090$ from the last scattering surface (LSS) using Eq. (D2):

$$\frac{\sigma_{D_A(1090)}}{D_A(1090)} = 0.001 \tag{D3}$$

-	n_s	w_0	w_a	Ω_b	Ω_K	$\Omega_{\rm cdm}$	h	σ_8
n_s	1.995792e+05	-3.736675e+04	-1.049368e+04	1.399776e+06	5.586439e+05	1.911997e+06	-7.651819e+04	-2.238062e+03
w_0	-3.736675e+04	1.839286e+05	5.165256e+04	-7.420507e+06	-3.987583e+06	-1.252519e+07	1.324383e+06	-4.515591e+02
w_a	-1.049368e+04	5.165256e+04	1.450555e+04	-2.083896e+06	-1.119830e+06	-3.517442e+06	3.719258e+05	-1.268110e+02
Ω_b	1.399776e+06	-7.420507e+06	-2.083896e+06	3.649438e+08	1.585996e+08	5.661366e+08	-5.168785e+07	3.203389e+04
Ω_K	5.586439e+05	-3.987583e+06	-1.119830e+06	1.585996e+08	8.705355e+07	2.705270e+08	-2.917404e+07	1.884381e+04
$\Omega_{\rm cdm}$	1.911997e+06	-1.252519e+07	-3.517442e+06	5.661366e+08	2.705270e+08	9.116277e+08	-8.940715e+07	6.346286e+04
h	-7.651819e+04	1.324383e+06	3.719258e+05	-5.168785e+07	-2.917404e+07	-8.940715e+07	9.889490e+06	-1.018381e+04
σ_8	-2.238062e+03	-4.515591e+02	-1.268110e+02	3.203389e+04	1.884381e+04	6.346286e+04	-1.018381e+04	1.517096e+04

Table D1. Plank's prior matrix corresponds to the cosmological parameters of interest.